Investigating the Role of the Tibetan Plateau in the Formation of Pacific Meridional Overturning Circulation

QIN WEN AND HAIJUN YANG

Laboratory for Climate and Ocean-Atmosphere Studies and Department of Atmospheric and Oceanic Sciences, School of Physics, Peking University, Beijing, China

ABSTRACT

The effects of the Tibetan Plateau (TP) on the Pacific Ocean circulation are investigated using a fully coupled climate model. Sensitivity experiments are designed to demonstrate that the presence of the TP is the reason for the lack of strong deep water formation in the subpolar North Pacific, because removing the TP in the model would enable the establishment of the Pacific meridional overturning circulation (PMOC). The processes involved are described in detail as follows. Removing the TP in the model would excite an anomalous high pressure over the subpolar North Pacific, causing anomalous Ekman downwelling that enhances surface water subduction north of 40°N. Removing the TP would also lead to less freshwater flux into the western Pacific, increasing sea surface salinity over the region. The high-salinity surface water can then be advected northward and eastward by the Kuroshio and its extension, subducting along the $26\text{–}27\sigma_\theta$ isopycnal surfaces to the deeper ocean, which enables the formation of deep water in the North Pacific and the setup of the PMOC. Afterward, more high-salinity warm water would be transported from the tropics to the extratropics by the Kuroshio, leading to the establishment of the PMOC. The role of the Rocky Mountains is also examined in this study. We conclude that the Rocky Mountains may play a trivial role in modulating the meridional overturning circulations in both the Pacific and Atlantic Oceans.

1. Introduction

The Tibetan Plateau (TP) is the highest and most extensive plateau in the world. The significant uplift of the TP can be traced back to 10–8 Ma (million years ago) (Harrison et al. 1992; Molnar et al. 1993). This uplift led to an enhanced aridity in the Eurasian interior and northern Great Plains (Ruddiman and Kutzbach 1989) and to vegetation changes from forests to grass land in Pakistan (Cerling et al. 1997) and along the northeastern margin of the TP (Ma et al. 1998). The TP uplift is also thought to be responsible for the peak dust transport to the North Pacific Ocean about 8–7 Ma (Rea et al. 1998). This accumulated dust over the Pacific could have resulted in more precipitation and low clouds by providing more nuclei of condensation to the atmosphere, leading to freshening and cooling of the North Pacific. Paleoclimatic evidence shows a possible strong North

Pacific Deep Water (NPDW) formation between 70–30 Ma and a diminishing NPDW since 30 Ma. The NPDW has nearly disappeared since 10 Ma (Ferreira et al. 2018, and references therein), the timing of which was consistent with that of the rapid TP uplift.

The influence of the TP on atmospheric circulations has received extensive attention since the 1950s (Flohn 1957). Model results show that the elevation increase along the TP and Himalayan areas is sufficient to alter thermally forced atmospheric circulations and establish strong continent-scale monsoons (Wu 1999; Wu et al. 2012; An et al. 2001; Chou and Neelin 2001; Wang 2006). Reducing the orography in the Northern Hemisphere (NH) can lead to more zonally oriented midlatitude westerly wind (Manabe 1974) and increase global surface temperature (Kutzbach et al. 1993; Kitoh 1997). Sensitivity experiments by Lee et al. (2013) showed that the TP tends to intensify the upper-level jet and stationary waves (both the Siberian high and Aleutian low), as well as the baroclinity in the North Pacific Ocean. Many model simulations have been used to investigate the effect of mountain uplift on the atmosphere–ocean system, including the Gulf Stream, the Humboldt Current, and El

---

Corresponding author: Haijun Yang, hjyang@pku.edu.cn

Niño–Southern Oscillation (Seager et al. 2002; Sepulchre et al. 2009; Feng and Poulsen 2014; Naiman et al. 2017).

Attention to the TP has never waned because of its huge thermal and dynamical effects on global climate. However, studies of TP impacts on global ocean circulations only emerged in the last 20 years as a result of the development of coupled atmosphere–ocean models (Kitoh 1997, 2002; Fallah et al. 2016; Maffre et al. 2018; Su et al. 2018). Many studies show that the present-day configuration of mountains forces the thermohaline circulation toward its modern state, that is, deep water formation in the North Atlantic Ocean, whereas it would have occurred in the Pacific in a flat world (Schmittner et al. 2011; Sinha et al. 2012); freshwater input is thought to be a major driver. Schmittner et al. (2011) and Sinha et al. (2012) found that the absence of higher mountains such as the Rocky Mountains can increase the moisture transport from the Pacific to the Atlantic, contributing to the increased salinity and enhanced deep water formation and meridional overturning circulation (MOC) in the Pacific and the decreased salinity and reduced deep water formation and MOC in the Atlantic. Maffre et al. (2018) reported that, in a world with a globally flat continent, the collapse of the Asian summer monsoon, associated with westward freshwater transport across Africa, is critical to the freshening of the Atlantic and the increased salinity in the Pacific. These studies suggested that continental topography is critical to the global thermohaline circulation. Modern-day topography may determine the formation of the deep MOC in the Atlantic and the lack of a deep MOC in the Pacific. However, these studies did not show individual roles of different mountains in shaping the modern-day MOC. Particularly, the role of the TP in the formation of global thermohaline circulation has not been fully investigated.

This work is a part of our series on the role of the TP in the formation of global MOC. In an accompanying paper, we investigate the TP's role in the formation of the Atlantic MOC (AMOC) (Yang and Wen 2019). This paper focuses on the Pacific MOC (PMOC). In a modern climate system, the Pacific features shallow wind-driven circulations, also called the subtropical cells (STCs) (e.g., Schott et al. 2004). Also, there is a lack of deep water formation in the subpolar North Pacific. Through sensitivity experiments of a fully coupled climate system model, we find that a deep MOC can develop in the Pacific when the TP is removed. In other words, the presence of the TP may be a critical background for the lack of the PMOC, and thus the existence of the AMOC (Yang and Wen 2019). The formation mechanism of the PMOC in the absence of the TP involves both wind-driven dynamics and thermohaline

dynamics. The combined effect of enhanced Ekman downwelling and denser surface water (mainly due to more saline water) subduction enables a strong deep water formation in the North Pacific, and thus the establishment of the PMOC. Our coupled model results may provide an explanation for the PMOC disappearance during the Late Miocene (12–9 Ma) when the accelerated uplift of the TP occurred (Woodruff and Savin 1989; von der Heydt and Dijkstra 2006) based on paleoclimatic records.

This paper is organized as follows. An introduction to the model and experiments used is given in section 2. Transient and equilibrium responses of the PMOC are presented in section 3. Atmospheric responses are described in section 4. Mechanisms for PMOC evolution are analyzed in section 5. The impact of the Rocky Mountains is shown in section 6. A summary and discussion are given in section 7.

2. Model and experiments

The Community Earth System Model (CESM1.0) of the National Center for Atmospheric Research is used in this study. CESM is a fully coupled global climate model that provides state-of-the-art simulations of Earth's past, present, and future climate states. The five components of CESM1.0 are the Community Atmosphere Model (CAM5; Park et al. 2014), the Community Land Model (CLM4; Lawrence et al. 2012), the Community Ice Code (CICE4; Hunke and Lipscomb 2010), the Parallel Ocean Program (POP2; Smith and Gregory 2009), and the Community Ice Sheet Model (Glimmer-CISM). The model grid employed in this study is T31_gx3v7. The CAM5 has 26 vertical levels, with the finite-volume nominal $3.75° \times 3.75°$ grid. The CLM4 has the same horizontal resolution as the CAM5. The POP2 has 60 vertical levels and a uniform 3.6° spacing in the zonal direction. In the meridional direction, the grid is nonuniformly spaced: It is 0.6° near the equator, gradually increasing to the maximum 3.4° at 35°N/S and then decreasing poleward. The CICE4 has the same horizontal grid as the POP2. No flux adjustments are used in CESM1.0.

To investigate the role of the TP in the formation of the PMOC, a 2400-yr control run and a 400-yr sensitivity run without the TP were carried out (Fig. 1). The control run, named "Real," starts from rest with standard configuration and a preindustrial carbon dioxide (CO_2) concentration of 285 ppm. The model geometry, topography, and continents of Real are realistic (Fig. 1a). The model climate in Real reaches quasi equilibrium after 1000 years of integration (Yang et al. 2015). The experiment without the TP, named "NoTibet," starts
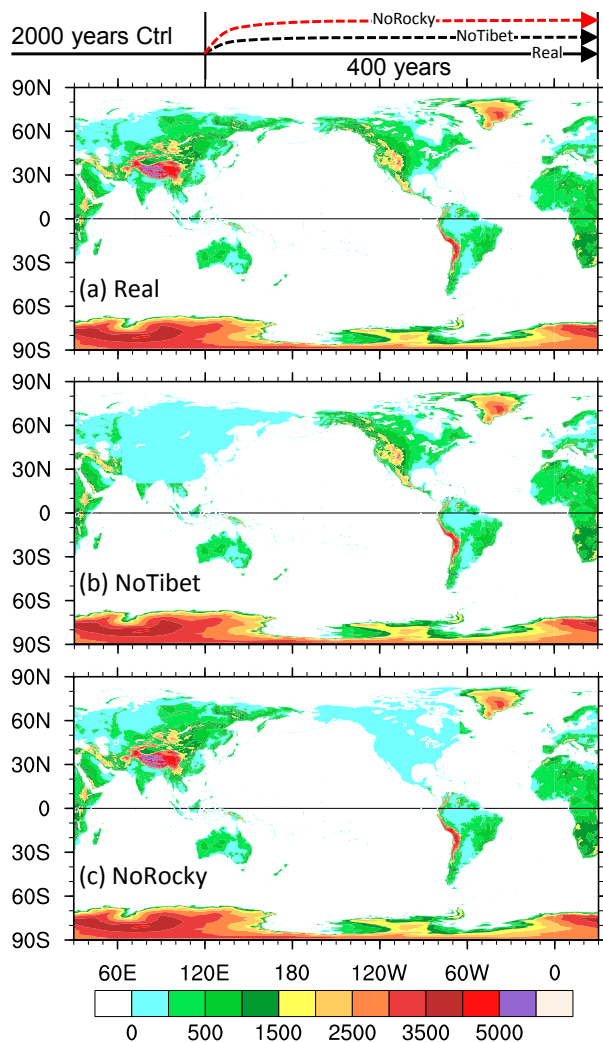
FIG. 1. Topography configuration (m) in coupled experiments: (a) the realistic topography used in the control simulation Real, (b) the modified topography without the Tibetan Plateau used in the experiment NoTibet, and (c) the modified topography without the Rocky Mountains used in the experiment NoRocky. The schematic at the top shows the integration lengths of these experiments.

from year 2001 of Real and is integrated for 400 years with the topography of the TP set at 50 m above sea level (Fig. 1b). In addition, we conducted 10 ensemble runs to minimize the effect of model internal variability on the transient change of the PMOC. These ensemble runs were integrated for 100 years each, having exactly the same configuration as NoTibet but starting from different years of Real around model year 2001. To compare the TP with other giant topography, we also conducted an experiment without the Rocky Mountains (RM), named "NoRocky" (Fig. 1c). NoRocky is run similarly as NoTibet, except that the topography of the RM is set at 50 m above the sea level. All other boundary

conditions in NoTibet and NoRocky, such as continent and ocean distribution, vegetation types, rivers, and orbital parameters, are the same as those in Real. For the regions with modified orography, the surface roughness parameters and gravity wave drag parameterization are set to be those for flat land. In the following discussion, the climate change due to the TP (RM) removal is obtained by subtracting the results of Real from those of NoTibet (NoRocky). The quasi-equilibrium change in a topography experiment is defined as the change averaged over the last 100 years of the 400-yr integration with respect to the control (Real).

3. Changes of PMOC

Removing the TP enables the establishment of the PMOC and the collapse of the AMOC. Figure 2a shows the temporal evolutions of both PMOC and AMOC in NoTibet and NoRocky, respectively. The PMOC and AMOC indices are defined as the maximum streamfunction in the range of 0°–10°C over 20°–70°N in the Pacific and Atlantic, respectively. We can see clearly in NoTibet that the PMOC (solid black curve) increases gradually during the first 150 years with a peak value of about 15 Sv ($1 Sv \equiv 10^6 m^3 s^{-1}$) and then declines slightly to reach a quasi-equilibrium state of about 10 Sv in about 300 years. The increase of the PMOC during the first 100 years is validated by 10 ensemble runs (gray curves in Fig. 2a), ensuring that it is a robust climate response. In comparison, the AMOC index shows more complicated evolution, which is strengthened during the first 50 years and then decreases linearly during the following 200 years; this is investigated in detail in Yang and Wen (2019). As shown in Fig. 2, removing the TP leads to a Pacific–Atlantic seesaw in terms of MOCs. Note that, different from previous studies (e.g., Schmittner et al. 2011), removing the RM does not cause significant changes in the MOCs (light-blue curves in Fig. 2a). In NoRocky, the PMOC is nearly unchanged and the AMOC only declines slightly (about 3 Sv) during the first 100 years and then recovers, suggesting that the RM is not a main driver for the Pacific–Atlantic seesaw in our experiments. In Schmittner et al. (2011), the RM were thought to be responsible for blocking atmospheric moisture transport from the Pacific to the Atlantic, so they played a role in the Pacific–Atlantic seesaw change. We will provide more details on this in section 6.

Spatial patterns of the MOC changes averaged in the quasi-equilibrium period are shown in Figs. 2b and 2c. In response to the TP removal, the PMOC and AMOC exhibit opposite responses, with a significant strengthening of downward mass transport in the subpolar North Pacific and a significant weakening of downward mass
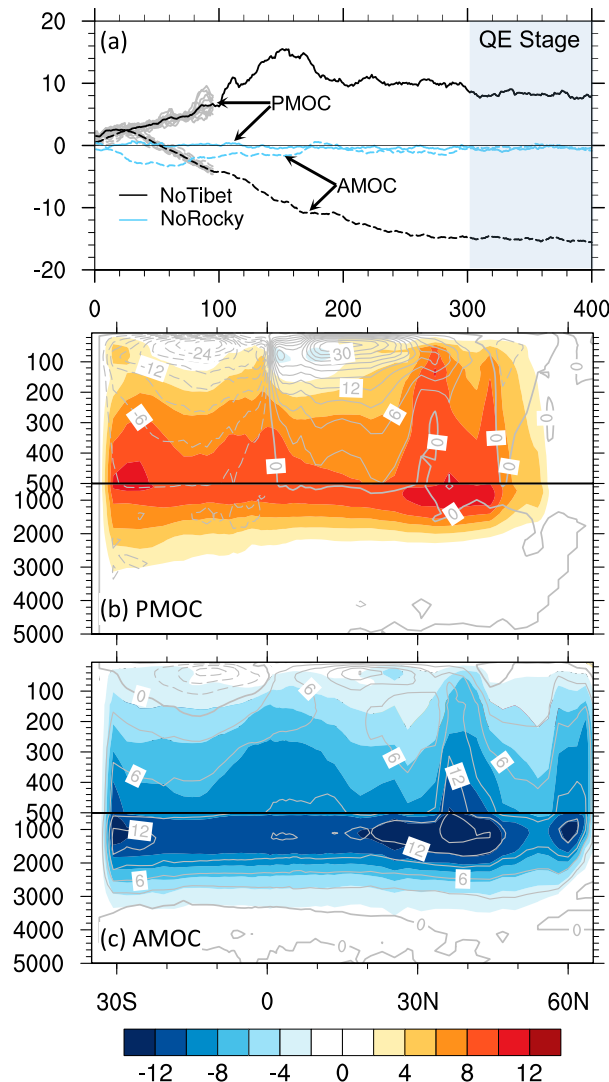
FIG. 2. (a) Temporal evolutions of the PMOC (solid) and AMOC (dashed) in NoTibet (black) and NoRocky (blue). The PMOC and AMOC indices are defined as the maximum streamfunction in the range of 0°–10°C between 20° and 70°N in the Pacific and Atlantic, respectively. Gray curves show the PMOC and AMOC changes in 10 ensemble runs in NoTibet. The quasi-equilibrium stage (shadow zone) is defined by year 300–year 400 in the experiment. Also shown are mean (b) PMOC and (c) AMOC (contours; Sv) in Real and its quasi-equilibrium change (colors) in NoTibet (with respect to Real). The MOC includes the effects of mesoscale (Gent–McWilliams) and sub-mesoscale mixing.

transport in the subpolar North Atlantic. The PMOC and AMOC responses are comparable in terms of magnitude. The depth of maximum PMOC change occurs at about 1000 m, slightly shallower than that of maximum AMOC change (1500 m). The PMOC change is confined to the south of 50°N while the AMOC change can extend to 60°N, indicating that the deep water

formation is generated at a lower latitude in the North Pacific than in the North Atlantic in response to the TP removal. Similar to the AMOC, the PMOC has an interhemispheric structure, suggesting its remarkable thermohaline component. It is worth noting that the MOC consists of both a wind-driven component and a thermohaline component (Weaver et al. 1993; Toggweiler and Samuels 1995). The shallow wind-driven MOCs (i.e., STCs) are confined mainly to the tropics. The Pacific STCs are much stronger than those of the AMOC (gray contours in the upper ocean in Figs. 2b and 2c). However, in both basins, the changes in STCs can be neglected (shading in the upper ocean in Figs. 2b and 2c).

Because of the seesaw changes in PMOC and AMOC, one can expect that the total MOC in global oceans would not change much. Figure 3 shows the mean global MOC (GMOC) in Real and NoTibet and its change in NoTibet. North of 30°S, similar patterns of GMOC in Real and NoTibet are due to the seesaw changes of the AMOC and PMOC (Figs. 3b,c). South of 30°S, the GMOC patterns are nearly identical, because the wind forcing over the Southern Ocean (SO) does not change much (Fig. 3a). The GMOC change in the SO is less than 4 Sv (Fig. 3d). Therefore, the contribution of wind forcing over the SO to the initial changes of the PMOC and AMOC in NoTibet can be neglected.

Bear in mind that the wind forcing over the SO is indeed critical to the GMOC, because the GMOC is thought to be maintained by the persistent Ekman pumping over the SO to a great extent (Toggweiler and Samuels 1995; Gnanadesikan 1999; Wunsch and Ferrari 2004; Nikurashin and Vallis 2012). In NoTibet, the persistent and stable Ekman pumping in the SO provides a necessary background condition that makes the full establishment of the PMOC possible. However, to start the PMOC, local buoyancy change in the North Pacific is crucial. In this work, we focus on the North Pacific, and emphasize that the PMOC is enabled by the surface buoyancy change in the North Pacific; the full establishment of the PMOC, however, has to rely on the persistent Ekman pumping in the SO. This may be the reason that, even after a 400-yr integration, the PMOC (Fig. 3c) is still weaker than the AMOC (Fig. 3b) by as much as 8 Sv (Fig. 3d), since the effect of Ekman pumping in the SO on the GMOC has a time scale of more than several hundred years. Recently, we integrated NoTibet to 1000 years, and the PMOC did become stronger in the later years (not shown).

The model experiments suggest an important role of the TP in the seesaw of the PMOC and AMOC. In our accompanying paper (Yang and Wen 2019) the TP effect on the AMOC is investigated in detail. In this paper, we focus on the TP effects on the PMOC and, in
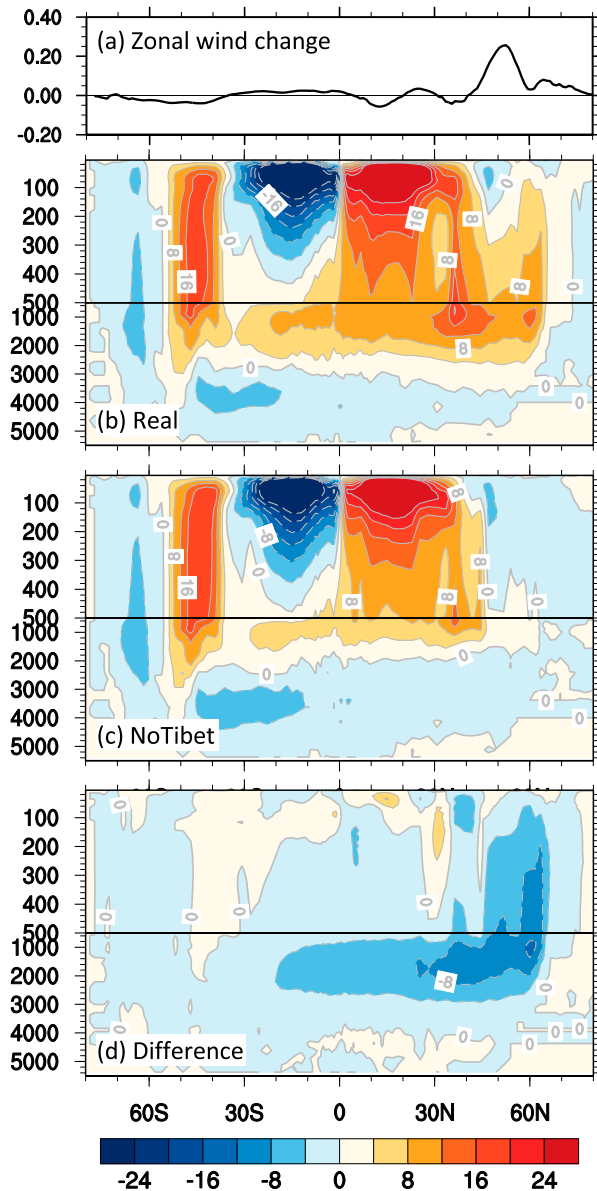
FIG. 3. (a) Quasi-equilibrium change in zonally averaged zonal-wind stress (dyn cm^{-2}), mean GMOC (Sv) in (b) Real and (c) NoTibet, and (d) quasi-equilibrium GMOC change in NoTibet (with respect to Real).

particular, the buoyancy change in the North Pacific that enables the PMOC. The role of the RM in global MOCs will be discussed briefly in section 6. The STCs are not discussed in this work since they appear to be insensitive to the TP removal.

4. Atmospheric responses

To understand the mechanism of the changes in the Pacific Ocean circulation, atmospheric responses are

examined first. It is well recognized that the impact of the TP can reach far beyond its immediate vicinity (Lee et al. 2013; Wu et al. 2015). Removing the TP leads to the genesis of low-level dipole anomalies near the TP, that is, a cyclonic and an anticyclonic circulations to the north and south of the TP, respectively (Fig. 4a). This dipole pattern of geopotential height change around the TP is a common feature in topography perturbation experiments (e.g., Brayshaw et al. 2009; White et al. 2017), which can be understood by using linear potential vorticity (PV) dynamics (Valdes and Hoskins 1991; White et al. 2017). In remote regions, an anomalous high pressure system is developed over the subpolar Pacific between 40° and 60°N, which is connected with the anomalous high south of the TP in the lower latitudes. This structure suggests a northeastward propagation of the group velocity of TP-generated Rossby wave. The atmospheric circulation changes over the Eurasian continent and Pacific Ocean in response to the TP removal fit the classical picture of topography-forced stationary wave (Valdes and Hoskins 1991; Lee et al. 2013) and can be well understood by the quasigeostrophic theory (Hoskins and Karoly 1981; Hoskins and Ambrizzi 1993). As part of the atmospheric circulation changes, the westerlies over the western and North Pacific become stronger and the trade winds over the tropical Pacific become weaker (Fig. 4a). The former make up the northern branch of the anomalous high over the North Pacific, while the latter are a manifestation of the attenuated Walker circulation that is due to the weakening of zonal Eurasia–Pacific thermal contrast (Fallah et al. 2016; Su et al. 2018).

Removing the TP leads to remarkable changes in the global hydrological cycle. The change in the atmospheric moisture transport suggests an enhanced freshwater flux from the western Pacific Ocean into the atmosphere (blue shading in Fig. 4b), which increases sea surface salinity (SSS) in the western and North Pacific (Fig. 6a1, described below). This is critical to the deep water formation in the North Pacific (details are given in Fig. 9, below). Since the moisture transport $\mathbf{v}q$ is determined by both atmospheric circulation $\mathbf{v}$ and specific humidity q, the $\mathbf{v}q$ pattern can be different from the circulation pattern shown in Fig. 4a. Note that, for a steady state, the vertically integrated moisture transport divergence $\nabla \cdot \mathbf{v}q$ of the entire atmosphere column is equivalent to the net freshwater flux across the ocean surface, that is, evaporation minus precipitation (EMP), when neglecting the freshwater flux of the land surface groundwater and river runoff (Yang et al. 2015). We plot the atmospheric moisture transport $\mathbf{v}q$ (vectors) and convergence $-\nabla \cdot \mathbf{v}q$ (shading) in Fig. 4b to better illustrate the connection of freshwater flux between
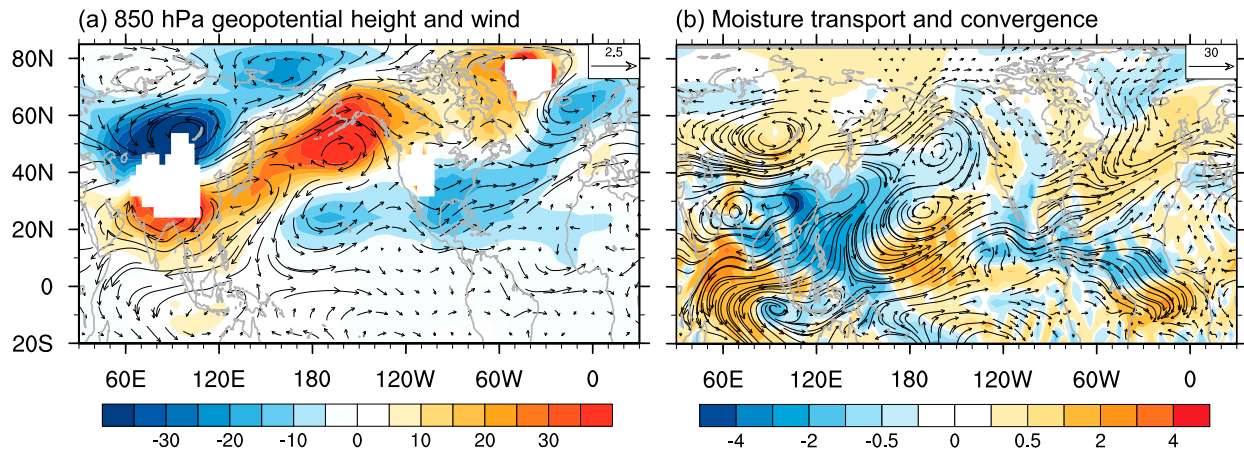
FIG. 4. Quasi-equilibrium changes in (a) geopotential height (shading; m) and wind (vectors; m s^{-1}) at 850 hPa, and (b) vertically integrated moisture transport ($\rho_a\mathbf{v}q$; vectors; kg m^{-1} s^{-1}) and its convergence [$-\rho_a\nabla \cdot (\mathbf{v}q)$; shading; 10^{-5} kg m^{-2} s^{-1}; positive for convergence and negative for divergence] in NoTibet (with respect to Real); $\rho_a = 1.29$ kg m^{-3} is mean air density. To see the wave structure more clearly, the zonal-mean geopotential height has been removed in (a).

different regions, and the freshwater exchange between ocean and atmosphere. The atmospheric moisture convergence is plotted as positive (i.e., $-\nabla \cdot \mathbf{v}q > 0$), representing a loss of atmosphere freshwater to the ocean (EMP < 0; i.e., $E < P$); the moisture divergence is plotted as negative, representing a loss of ocean freshwater to the atmosphere. Figure 4b shows the enhanced freshwater flux from the ocean into the atmosphere over the western tropical Pacific and North Pacific, leading to SSS increase there. The resulted high-salinity surface water can then be transported northward by the Kuroshio (KC) and farther eastward by the Kuroshio Extension (KE), which would enable the deep water formation in the North Pacific.

5. Changes in the Pacific Ocean

a. Surface buoyancy change

The surface ocean in the North Pacific warms up appreciably in response to the TP removal (Fig. 5a), which acts against the deep water formation and does not favor the thermohaline circulation in the Pacific. The temperature budget analysis reveals that the surface warming in the North Pacific is largely attributed to the weakened southward cold water advection through the Bering Strait (not shown) and the increased downward shortwave (SW) radiation (Fig. 5b). Note that the sea surface temperature (SST) warming in the Bering Sea is also related to the sea ice retreat over there. The sea ice shrinking in the Bering Sea, denoted by the sea ice margin in Fig. 5b, reduces surface albedo and thus increases the downward SW in the Bering Sea. Figure 5c shows the net incoming SW change that results from cloud radiation forcing,

which is mainly determined by low-cloud change (Fig. 5d). The reduced low cloud in the western and North Pacific is consistent with the divergence of moisture transport over these regions (Fig. 4b), that is, fewer low clouds corresponding to less precipitation and thus leading to more evaporation (EMP > 0).

In this work, more attention is paid to the ocean buoyancy change that can promote the deep water formation in the North Pacific. Figure 6 shows that it is the increase of SSS that increases the sea surface density (SSD) in the North Pacific. The transient response of SSS shows that high-salinity surface water forms in the western boundary region of the Pacific subtropical circulation, immediately after the TP removal (Fig. 6a1), where the remarkable divergence of atmospheric moisture transport occurs (Fig. 4b), as discussed in section 4. This high-salinity surface water is advected eastward by the KC and its extension, and relayed farther eastward by the North Pacific Current, contributing greatly to the SSS increase in the central and eastern North Pacific (Figs. 6a2,a3). The high-salinity surface water is further advected northward by the Alaska Coastal Current and southward by the California Coastal Current, along the west coast of North America, contributing greatly to the SSS increase in the subpolar Pacific and the subtropical eastern coastal ocean, respectively (Figs. 6a3,a4). The SSS change reaches its quasi-equilibrium in about 150 years. The high-salinity surface water finally occupies most regions of the North Pacific, providing a deterministic factor to the SSD change there. The transient change in SSD follows closely the change in SSS (Figs. 6b1–b4), showing widespread denser surface water occupying the North Pacific,
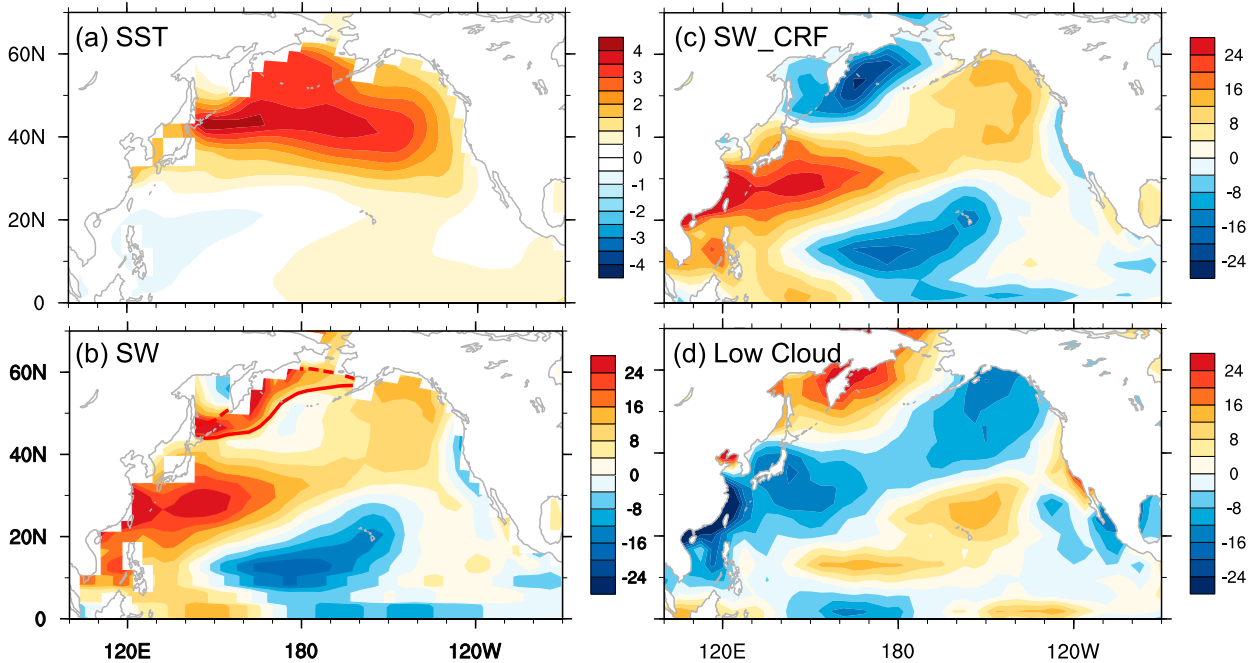
FIG. 5. Quasi-equilibrium changes in (a) SST (°C), (b) SW (W m^{-2}), (c) cloud radiation forcing of SW (W m^{-2}), and (d) percentage change of low cloud (%) in NoTibet (with respect to Real). Solid and dashed red curves in (b) denote the sea ice margin in Real and NoTibet, respectively, which is defined by the 15% sea ice fraction.

although the density increase has been partially offset by the SST increase. This SSD increase provides a critical condition for the deep water formation in the North Pacific, and thus enables the PMOC.

b. Dynamics of deep water formation

How and where the surface water sinks into the deeper ocean is closely related to ocean dynamics. We examine mixed layer depth (MLD) first, because it can signal to some extent where the surface water subduction occurs and how deep the surface water can go down. Figure 7 shows the change in March MLD, which is

calculated following Large et al. (1997). In the North Pacific, March MLD becomes significantly deeper in the western Pacific, the KE region, and the eastern subpolar Pacific after the TP removal, indicating where the enhanced subduction, vertical mixing, and diffusion occur. In comparison, the March MLD in the North Atlantic Deep Water (NADW) formation region becomes significantly shallower in NoTibet, which corresponds to AMOC shutdown (Yang and Wen 2019).

It is well known that in the present climate the Pacific is dominated by shallow wind-driven circulations, with weak thermohaline processes. However, in the world
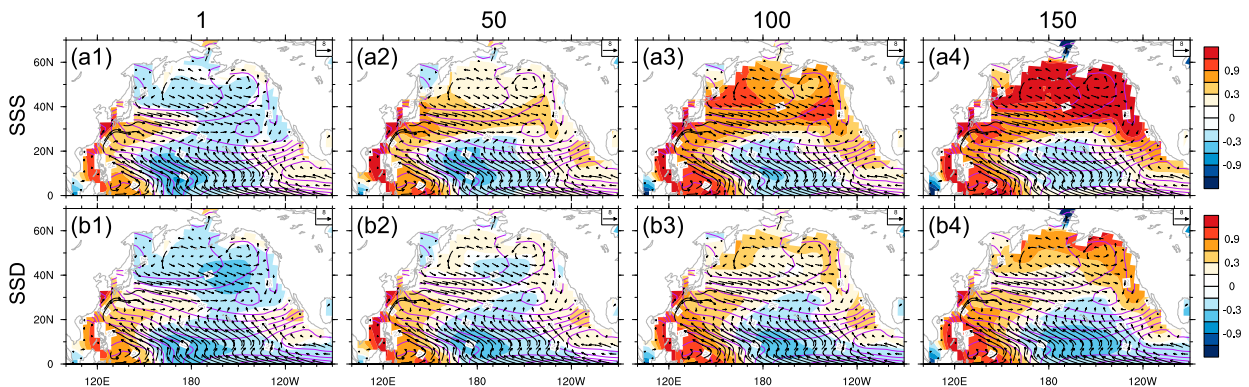

FIG. 6. Changes in (a) SSS (shading; psu) and (b) SSD (shading; kg m^{-3}) in years 1, 50, 100, and 150 of NoTibet (with respect to Real). The mean surface current and mean SSD in Real are superposed as vectors (m s^{-1}) and purple contours (kg m^{-3}), respectively.
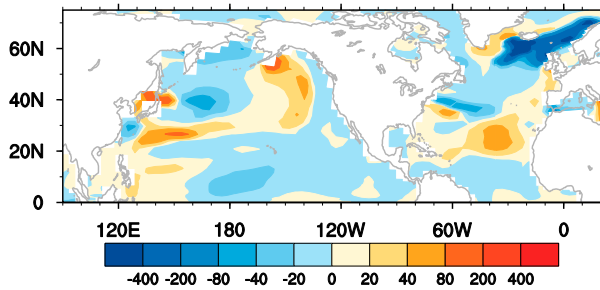
FIG. 7. Change of March mixed layer depth (MLD; m) in NoTibet (with respect to Real). The MLD is defined similarly as in Large et al. (1997).

FIG. 8. Climatological mean Ekman pumping (shading; cm day^{-1}; positive for upwelling and negative for downwelling), and potential vorticity (PV; gray contours; 10^{-10} m^{-1} s^{-1}) averaged between 26 and 27σ_θ in Real. Stippling indicates anomalous Ekman downwelling in NoTibet (with respect to Real). The purple dashed curve denotes the outcropping line of 26σ_θ. The thick gray line represents PV = 3 $\times$ 10^{-10} m^{-1} s^{-1}. The contour interval is 0.2 $\times$ 10^{-10} m^{-1} s^{-1} or 1 $\times$ 10^{-10} m^{-1} s^{-1} for PV smaller or larger, respectively, than 3 $\times$ 10^{-10} m^{-1} s^{-1}.

without the TP, the thermohaline processes would become important because there are more saline and denser surface waters, which can subduct into the deep ocean, even deeper with the help of enhanced Ekman downwelling. Their joint effect leads to the setup of the PMOC. The Ekman pumping in Real and its change in NoTibet are plotted in Fig. 8. Here, the Ekman pumping velocity ω_e is calculated by curl($\boldsymbol{\tau}/f)/\rho_0$, where $\boldsymbol{\tau} = (\tau^x, \tau^y)$ is surface wind stress vector, f is the Coriolis parameter, and ρ_0 is the mean seawater density. In the present climate, there are upwelling in the subpolar ocean and downwelling in the subtropics generally (shading in Fig. 8). The mean downwelling in the subtropics is about 30 m yr^{-1}. When the TP is removed, anomalous Ekman downwelling occurs in the subpolar region, the western subtropical Pacific, and the eastern subtropical coastal ocean (stippling in Fig. 8), with a magnitude of about 10 m yr^{-1}. There is about 30% enhancement of the mean downwelling with respect to that in Real. These anomalous downwelling regions are forced by the anomalous high pressure systems above (Fig. 4a), which encourage the vertical mixing and subduction process.

In fact, the denser surface water in NoTibet enters the ocean interior through the so-called ventilation window, denoted by the outcropping line of 26σ_θ (dashed purple curve in Fig. 8), and subducts eastward, downward, and equatorward. The 26σ_θ line is chosen because it is located along the northern edge of anomalous high-saline surface water in the western Pacific (Fig. 6a1). The subduction passage is roughly determined by mean PV (Schneider et al. 1999; Stephens et al. 2001). In Fig. 8, we plot the mean PV averaged over the 26–27σ_θ isopycnals (solid gray contours). The mean PV is calculated using $(\Delta\rho/\rho_0)(f/\Delta H)$, where $\Delta\rho = 1$ and ΔH is the layer thickness between 26 and 27σ_θ levels. The PV contours, say, the contours of 1.6–2.2, emanate from the outcropping window of 26σ_θ in the western Pacific to the eastern Pacific, suggesting an eastward and downward
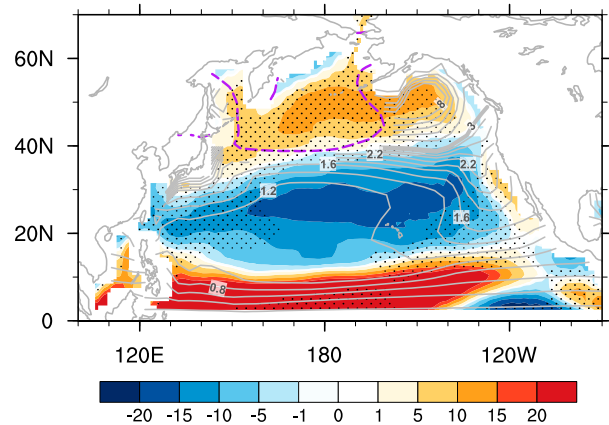
subduction of denser surface water. In the eastern Pacific, the 1.6–2.2-PV contours go southward, suggesting farther southward and downward subduction.

The subduction process in the North Pacific after the TP removal is illustrated more clearly in Fig. 9, with the three-dimensional structure of salinity anomalies. Figures 9a1–a4 are zonal sections of salinity changes along 40°–45°N, the latitudes of the KE and the North Pacific Current, superposed by mean isopycnal contours. They show clearly that the high-salinity surface water goes eastward and downward mainly within the 26–27σ_θ levels and eventually reaches about 1000 m in the eastern Pacific in 150 years (Fig. 9a4). There is also a local deep penetration of high-salinity surface water near the western boundary (Figs. 9a1,a2), which occurs rapidly and can reach about 1500 m in 50 years (Fig. 9a2), much faster than the eastward subduction process. This also contributes to the setup of the PMOC. Figures 9b and 9c are meridional sections of salinity changes averaged in the western Pacific (135°–150°E) and eastern Pacific (170°E–120°W), respectively. The downward high-salinity water in the western Pacific affects the deep ocean mainly through diapycnal mixing and diffusion (Fig. 9b), fostered by anomalous surface Ekman downwelling (Fig. 8). In comparison, the high-salinity water in the eastern Pacific reaches the deep ocean mainly along the isopycnals between 26 and 27σ_θ (Figs. 9c2–c4), which is much stronger and reaches deeper than that in the western Pacific (Fig. 9c4 versus Fig. 9b4). Both the western and eastern Pacific subduction can reach
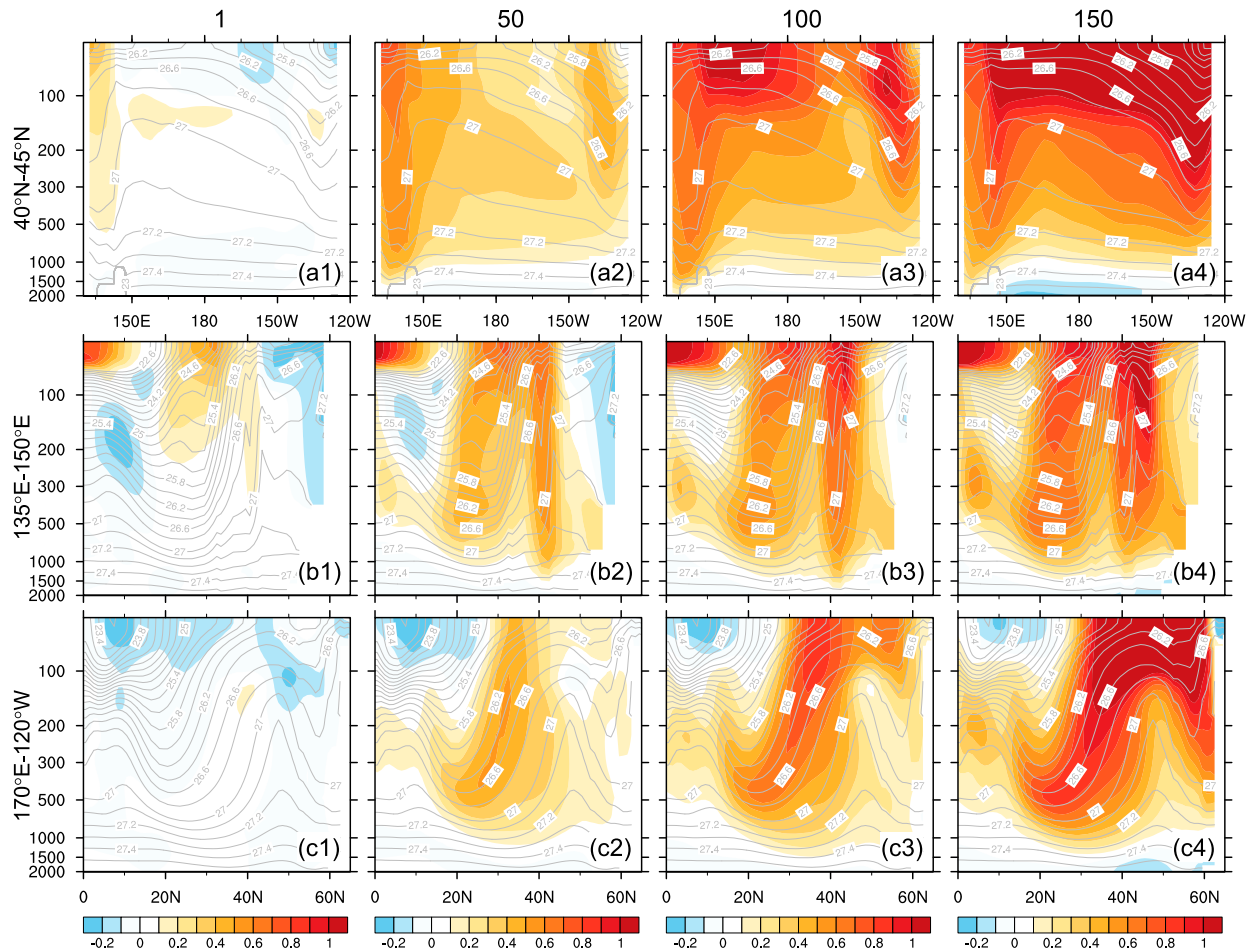
FIG. 9. Changes in ocean salinity (shading; psu) in the North Pacific in years 1, 50, 100, and 150 of NoTibet (with respect to Real). The mean ocean density (kg m^{-3}) in Real is superposed as gray contours. Shown are depth–longitude sections averaged over (top) 40°–45°N, (middle) the western Pacific (135°–150°E), and (bottom) the eastern Pacific (170°–120°W).

the equatorial thermocline. The three-dimensional structure of the salinity change is consistent with the PV dynamics shown in Fig. 8.

In summary, when the TP is removed, the high-salinity surface water forms in the western and North Pacific due to less precipitation and enhanced evaporation. This increases SSD in these regions. The denser surface water is transported eastward by the KE and North Pacific Current, subducting into the deep ocean along the pathway determined by mean PV. The denser surface water can reach beyond 1500 m in depth, which triggers the setup of the PMOC. In fact, once the PMOC starts, the KC and its extension will be enhanced, which furthers the subduction processes in the North Pacific. There is a positive feedback among the PMOC, KC, SSS, and the subduction processes. The NPDW formation also involves wind-driven dynamics. This is different from that in the North Atlantic, where only the thermohaline process plays the critical role.

Since the wind-driven dynamics has a shorter time scale, the PMOC develops much more quickly than the AMOC slows down (Fig. 2a). The PMOC reaches its peak strength in about 150 years when the AMOC is only weakened by 50%.

6. Role of the Rocky Mountains

To further understand the role of the TP in global MOCs, we examine the role of the RM briefly in this section. The RM are located between the Pacific and Atlantic with great height and extension. What is the role of the RM in global MOCs, and how does that compare with the TP's role? An earlier study by Warren (1983) suggested that since the presence of the RM contributes greatly to the wind climatology over the North Atlantic, the wind-driven northward salt transport in the North Atlantic is more efficient than that in the North Pacific, which results in stronger sinking in the North

Atlantic. Therefore, the RM plays a role in the formation of the AMOC. A recent study by Schmittner et al. (2011) suggested that the presence of the RM might be a reason for the deep water formation occurring in the Atlantic rather than in the Pacific, because the RM can block the atmospheric moisture transport from the North Pacific to the North Atlantic. Note that these two mechanisms are different. In our experiment of NoRocky, however, the RM do not play a role in either AMOC formation or PMOC destruction (light-blue curves in Fig. 2a), dramatically different from the findings of these previous studies.

The changes in atmospheric circulations around the RM region in NoRocky (Fig. 10a) are similar to those around the TP in NoTibet (Fig. 4a); that is, there are cyclonic and anticyclonic circulations developing to the north and south of the removed RM, respectively. The cyclonic anomaly extends from the northwest of the RM to the eastern Pacific, and the anticyclonic anomaly extends from the North American continent to the sub-polar North Atlantic. These atmospheric changes cause atmospheric moisture divergence over most of the North Atlantic (Fig. 10b), which tends to increase the SSS there. In addition, the atmospheric circulation change causes anomalous Ekman downwelling in the North Atlantic and Ekman upwelling in the northeast Pacific (Fig. 10c). Figure 10 implies that in the *presence* of the RM, the atmosphere circulation and moisture transport do not favor a saline surface ocean in the North Atlantic or strong NADW formation.

Figure 11 shows the quasi-equilibrium change of surface buoyancy in the Pacific and Atlantic in response to the RM removal. It is straightforward: that is, the SSD increase in the northeastern coastal Pacific (Fig. 11c1) is contributed by colder SST (Fig. 11a1) and higher SSS (Fig. 11b1), while the SSD decrease in the North Atlantic is contributed by warmer SST and lower SSS. The surface cooling in the North Pacific can only penetrate downward to a depth of 500 m along $26.2\sigma_\theta$ (Fig. 11a2). The high-salinity coastal water along the eastern coastal Pacific (Fig. 11b1) is confined above the 200-m depth (Fig. 11b2). Given the anomalous Ekman pumping in the North Pacific (Fig. 10c), the subduction of the denser surface water along the $26.2\sigma_\theta$ isopycnal is weak and can only reach ~300 m (Fig. 11c2). This shallow subduction is far from sufficient to form the NPDW and thus unable to start the PMOC. In the North Atlantic, the warmer and fresher surface water (Figs. 11a1,b1) reduces the NADW formation to some extent (Figs. 11c1,c3), which leads to a slight decline in the AMOC in the transient period of NoRocky (dashed blue curve, Fig. 2a). It is seen that warm surface anomaly can penetrate downward to about 1000 m (Fig. 11a3),
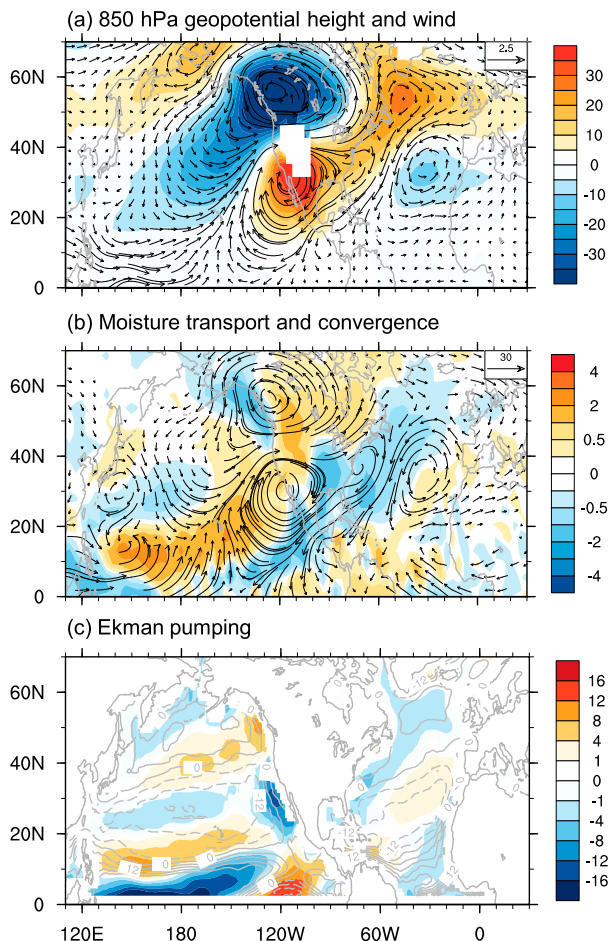

(a) 850 hPa geopotential height and wind

(b) Moisture transport and convergence

(c) Ekman pumping

FIG. 10. Quasi-equilibrium changes in (a) geopotential height (shading; m) and wind (vectors; m s^{-1}) at 850 hPa, (b) vertically integrated moisture transport (vector; kg m^{-1} s^{-1}) and its convergence ($-\rho_a\nabla \cdot \mathbf{v}q$; shading; 10^{-5} kg m^{-2} s^{-1}; positive for convergence and negative for divergence), and (c) Ekman pumping velocity (shading; cm day^{-1}; positive for upwelling and negative for downwelling) in NoRocky (with respect to Real). In (c), the mean Ekman pumping of Real is plotted as gray contours (cm day^{-1}).

carried by the downward branch of the mean AMOC and fostered further by the anomalous Ekman downwelling (Fig. 10c). Note that the freshening occurs in the western North Atlantic and Labrador Sea, which is confined in the top ~200-m depth (Fig. 11b3). There is a weak SSS increase in the eastern North Atlantic (Fig. 11b1), which contributes to the deeper penetration near 40°N (Fig. 11b3). In general, the surface water in the North Atlantic becomes only slightly lighter (Fig. 11c1). This only leads to a weak reduction in the NADW formation (Fig. 11c3), which is far from effective to cause AMOC shutdown.

A brief summary about the role of the RM in MOCs is given here. Our model experiments show that in a world without the RM, the AMOC would not change much
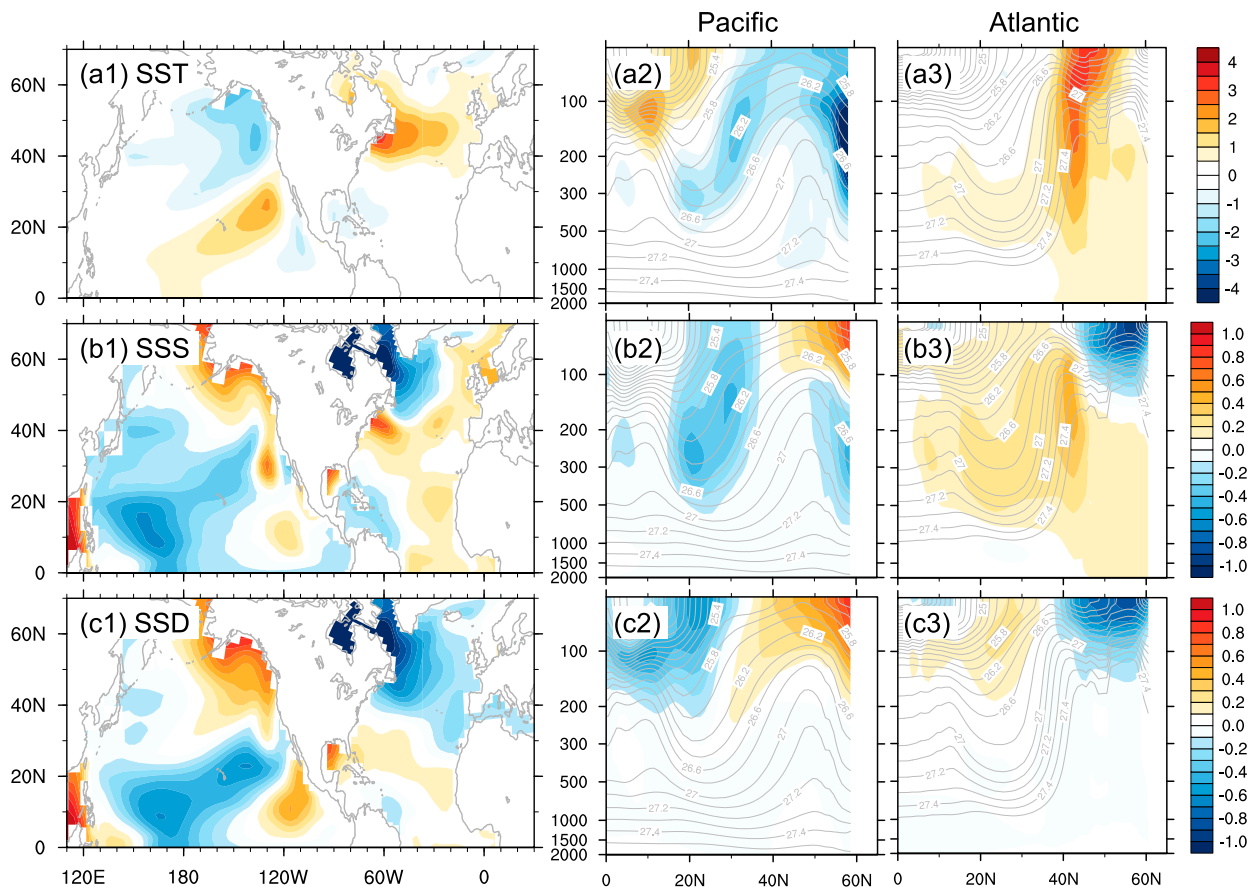
FIG. 11. Quasi-equilibrium changes in (a1) SST (shading; °C), and depth–latitude sections of temperature anomaly (shading; °C) averaged over (a2) 160°–140°W of the Pacific and (a3) 60°–40°W of the Atlantic in NoRocky (with respect to Real). In (a2) and (a3), the mean ocean density (kg m^{-3}) in Real is superposed as gray contours. Also shown as in (a) are (b) salinity (psu) and (c) density (kg m^{-3}). The panels in the same row share the same color scale.

and the PMOC would not occur. In other words, this work suggests that the presence of the RM may not be a factor contributing to the current reality that the deep overturning circulation occurs in the Atlantic instead of in the Pacific. This is different from the finding of Schmittner et al. (2011), which concluded that the RM can play a role because the presence of the RM blocks the atmospheric moisture transport from the North Pacific to the North Atlantic. In our study, removing the RM does lead to an enhanced moisture transport from the eastern Pacific to the eastern continental area of North America, roughly along the latitude of 50°N (Fig. 10b). However, there is also enhanced atmospheric moisture transport from the North Atlantic southwestward all the way to the eastern tropical Pacific (Fig. 10b). The second moisture transport pathway dominates over the first one, contributing to the SSS increase in the North Atlantic. In other words, our results suggest that although the *presence* of the RM blocks the zonal moisture transport from the North Pacific to the North

Atlantic, it also enhances the moisture transport from the eastern tropical Pacific to the North Atlantic. The latter effect is stronger than the former effect, eventually contributing to the freshening of the North Atlantic, instead of increasing SSS there. Warren (1983) concluded that the presence of the RM can lead to strong wind-driven northward salt transport in the North Atlantic. However, the strong atmospheric moisture transport from the eastern tropical Pacific to the North Atlantic tends to freshen the North Atlantic at the same time. We also examined the wind-driven salt transport in the North Atlantic in the presence of the RM (not shown). We found these two effects roughly cancel each other, leading to a trivial effect of the RM on the AMOC.

With regard to the mechanisms of SSS changes in both oceans, the atmospheric moisture transport and divergence/convergence (i.e., the net surface freshwater flux, or EMP) shown in Fig. 10b is just one factor. In fact, it is not even an important factor for the SSS change in the North Atlantic, because the SSS change shows a
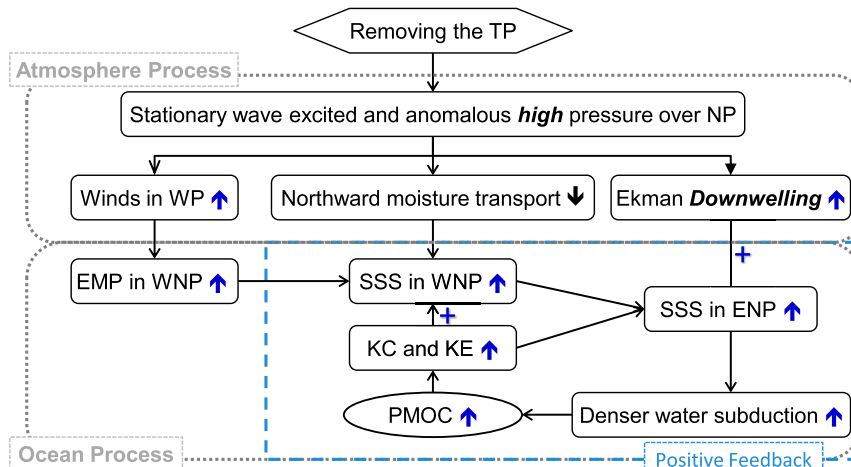
FIG. 12. Schematic diagram summarizing the main processes for PMOC setup after the TP is removed. Note that there is no causality between "Ekman downwelling" and "SSS in ENP." These two effects when combined can lead to more denser-water subduction in the North Pacific. The upward and downward arrows respectively represent increases and decreases. Acronyms used here are WP for western Pacific, NP for North Pacific, WNP for western North Pacific, and ENP for eastern North Pacific; the others are defined in the text.

general freshening in the western North Atlantic (Fig. 11b1) rather than an increase as suggested by the EMP change shown in Fig. 10b. The freshening in the western North Atlantic is mainly due to the southward sea ice expansion and melting along the eastern Greenland (not shown), which is also fostered by surface warming (Fig. 11a1). The surface warming in the North Atlantic (Fig. 11a1) is mainly contributed by enhanced SW radiation (not shown). Since this paper focuses mainly on the TP's effect on the PMOC, detailed diagnoses of the ocean changes resulting from the RM removal are not presented.

7. Summary and discussion

The role of the TP in the PMOC is investigated in this study. Through coupled model sensitivity experiments, we illustrate that an interhemispheric PMOC can develop after the TP is removed. The main processes related to the PMOC establishment are summarized in Fig. 12. When the TP is removed, a planetary wave train is excited immediately in the NH mid-to-high latitudes and an anomalous high pressure system develops over the subpolar North Pacific. This high pressure anomaly is accompanied by enhanced westerlies over the western and subpolar North Pacific. It also causes a weakened moisture transport from the western tropical Pacific to the North Pacific, and enhanced Ekman downwelling in the North Pacific. In response to these atmospheric changes, the surface ocean in the western Pacific becomes more saline, which increases the SSD there. The

denser surface water sinks in the western Pacific and is advected eastward by the KE and North Pacific Current, subducting downward and southward along an isopycnal surface. This denser surface water subduction is further enhanced by anomalous Ekman downwelling, and can reach as deep as 1500 m. This deep water formation process would finally lead to the establishment of the PMOC, during which the positive feedback among the Kuroshio and its extension, the northward and eastward saline water advection, and the denser surface water subduction play an important role (Fig. 12).

The presence of the TP may be a critical background for the global thermohaline circulation in the present climate, based on this work and our accompanying paper on the AMOC (Yang and Wen 2019). Paleoclimatic records have provided some evidence suggesting the seesaw change between the Pacific and Atlantic (Ferreira et al. 2018, and references therein), which may have occurred between 30 and 10 Ma. The mechanisms for the seesaw change include the Drake Passage opening in about 21 Ma (Toggweiler and Samuels 1995), the Bering Strait opening (Hu et al. 2012), the uplift of the RM (Schmittner et al. 2011), and so on. In this work, we propose that the uplift of the TP may be a key for the seesaw change, because the timing of the rapid uplift of the TP corresponded well to the timings of the strong NADW formation and diminished NPDW (about 10 Ma) (Woodruff and Savin 1989; Harrison et al.1992; Molnar et al. 1993). In contrast, the RM had reached its modern elevation by ~45 Ma. Although the RM helps block some moisture transport from the

North Pacific to the North Atlantic, it also enhances the northeastward atmosphere moisture transport from the eastern tropical Pacific to the North Atlantic. Paleoclimatic evidence does not support a strong NADW formation around 45 Ma when the RM reached its modern-day height (Hohbein et al. 2012; Boyle et al. 2017). Our sensitivity experiment suggests no remarkable changes in the deep water formation in both Pacific and Atlantic after the RM is removed.

In this study, the topography experiments are only integrated for 400 years, which might not be long enough for the full adjustment of global ocean circulations. Particularly, the full establishment of the PMOC will have to be connected with the persistent Ekman pumping in the SO (Toggweiler and Samuels 1995; Gnanadesikan 1999; Wunsch and Ferrari 2004; Nikurashin and Vallis 2012). The effect of Ekman pumping in the SO on the GMOC has a time scale of more than several hundred years, which requires a much longer model integration. This also raises a critical question: Would the states of PMOC and AMOC be the same in 4000 years as those in 400 years? A recent study by Jansen et al. (2018) found that the transient and equilibrium responses of the AMOC to warming can be dramatically different. Their model experiment was integrated for more than 10 000 years. The transient AMOC shows significant weakening, whereas the equilibrium AMOC shows strengthening. Very recently, we integrated NoTibet to 1400 years. The AMOC and PMOC respectively remain in "off" and "on" states for 1000 years. The AMOC is always stable, whereas the PMOC in the later stage becomes stronger. Fortunately, so far the changes of the AMOC and PMOC in NoTibet do not show multi-equilibrium states. This paper focuses on the mechanisms that start the PMOC, so analyzing the results from a 400-yr experiment should be adequate. Nevertheless, experiments with longer integration are needed.

We are aware that the results from these extreme orographic forcing experiments may not be comparable to observed features. However, they are helpful for a better understanding of detailed processes related to dramatic topography changes. Quantifying the impact of TP uplift on global ocean circulations is difficult in a realistic world, although there are observations and model results showing qualitatively the connection between large-scale ocean circulation changes and tectonic changes in the Miocene (Barker and Burrell 1977; Kennett 1977). It is also possible that the conclusions drawn in this study are model dependent and that they are subject to model limitations. In this work, the model resolutions for both ocean and atmosphere components are coarse; particularly, the ocean model used here cannot fully resolve the convection in the Labrador Sea. Moreover, the model experiments are performed with constant atmospheric CO_2 concentration at the preindustrial level, whereas the concentration was higher during the TP uplift phase in the real world. For example, in the Late Eocene the climate conditions were accompanied by high atmospheric CO_2 concentration (Lowenstein and Demicco 2006), which might have influenced the sea ice state to a great extent. Studies using different models, or the same model with various background climate parameters, are needed for a better understanding of the TP's role in shaping global ocean circulations.

REFERENCES

An, Z., J. E. Kutzbach, W. Prell, and S. Porter, 2001: Evolution of Asian monsoons and phased uplift of the Himalaya-Tibetan plateau since Late Miocene times. *Nature*, **411**, 62–66, https://doi.org/10.1038/35075035.

Barker, P. F., and J. Burrell, 1977: The opening of Drake Passage. *Mar. Geol.*, **25**, 15–34, https://doi.org/10.1016/0025-3227(77)90045-7.

Boyle, P. R., B. W. Romans, B. E. Tucholke, R. D. Norris, S. A. Swift, and P. F. Sexton, 2017: Cenozoic North Atlantic deep circulation history recorded in contourite drifts, offshore Newfoundland, Canada. *Mar. Geol.*, **385**, 185–203, https://doi.org/10.1016/j.margeo.2016.12.014.

Brayshaw, D. J., B. Hoskins, and M. Blackburn, 2009: The basic ingredients of the North Atlantic storm track. Part I: Land–sea contrast and orography. *J. Atmos. Sci.*, **66**, 2539–2558, https://doi.org/10.1175/2009JAS3078.1.

Cerling, T. E., J. M. Harris, B. J. MacFadden, M. G. Leakey, J. Quade, V. Eisenmann, and J. R. Ehleringer, 1997: Global vegetation change through the Miocene/Pliocene boundary. *Nature*, **389**, 153–158, https://doi.org/10.1038/38229.

Chou, C., and J. D. Neelin, 2001: Mechanisms limiting the southward extent of the South American summer monsoon. *Geophys. Res. Lett.*, **28**, 2433–2436, https://doi.org/10.1029/2000GL012138.

Fallah, B., U. Cubasch, K. Prömmel, and S. Sodoudi, 2016: A numerical model study on the behaviour of Asian summer monsoon and AMOC due to orographic forcing of Tibetan Plateau. *Climate Dyn.*, **47**, 1485–1495, https://doi.org/10.1007/s00382-015-2914-5.

Feng, R., and C. J. Poulsen, 2014: Andean elevation control on tropical Pacific climate and ENSO. *Paleoceanography*, **29**, 795–809, https://doi.org/10.1002/2014PA002640.

Ferreira, D., and Coauthors, 2018: Atlantic–Pacific asymmetry in deep-water formation. *Annu. Rev. Earth Planet. Sci.*, **46**, 327–352, https://doi.org/10.1146/annurev-earth-082517-010045.

Flohn, H., 1957: Large-scale aspects of the summer monsoon in South and East Asia. *J. Meteor. Soc. Japan*, **35A**, 180–186, https://doi.org/10.2151/jmsj1923.35A.0_180.

Gnanadesikan, A., 1999: A simple predictive model for the structure of the oceanic pycnocline. *Science*, **283**, 2077–2079, https://doi.org/10.1126/science.283.5410.2077.

Harrison, T. M., P. Copeland, W. S. Kidd, and A. Yin, 1992: Raising Tibet. *Science*, **255**, 1663–1670, https://doi.org/10.1126/science.255.5052.1663.

Hohbein, M. W., P. F. Sexton, and J. A. Cartwright, 2012: Onset of North Atlantic deep water production coincident with inception of the Cenozoic global cooling trend. *Geology*, **40**, 255–258, https://doi.org/10.1130/G32461.1.

Hoskins, B. J., and D. J. Karoly, 1981: The steady linear response of a spherical atmosphere to thermal and orographic forcing. *J. Atmos. Sci.*, **38**, 1179–1196, https://doi.org/10.1175/1520-0469(1981)038<1179:TSLROA>2.0.CO;2.

——, and T. Ambrizzi, 1993: Rossby wave propagation on a realistic longitudinally varying flow. *J. Atmos. Sci.*, **50**, 1661–1671, https://doi.org/10.1175/1520-0469(1993)050<1661:RWPOAR>2.0.CO;2.

Hu, A., G. A. Meehl, W. Han, A. Abe-Ouchi, C. Morrill, Y. Okazaki, and M. O. Chikamoto, 2012: The Pacific–Atlantic seesaw and the Bering Strait. *Geophys. Res. Lett.*, **39**, L03702, https://doi.org/10.1029/2011GL050567.

Hunke, E. C., and W. H. Lipscomb, 2010: CICE: The Los Alamos Sea Ice Model, documentation and software user's manual, version 4.1. Los Alamos National Laboratory Rep. LA-CC-06-012, 76 pp., https://csdms.colorado.edu/w/images/CICE_documentation_and_software_user%27s_manual.pdf.

Jansen, M. F., L. P. Nadeau, and T. M. Merlis, 2018: Transient versus equilibrium response of the ocean's overturning circulation to warming. *J. Climate*, **31**, 5147–5163, https://doi.org/10.1175/JCLI-D-17-0797.1.

Kennett, J. P., 1977: Cenozoic evolution of Antarctic glaciation, the circum-Antarctic Ocean, and their impact on global paleoceanography. *J. Geophys. Res.*, **82**, 3843–3860, https://doi.org/10.1029/JC082i027p03843.

Kitoh, A., 1997: Mountain uplift and surface temperature changes. *Geophys. Res. Lett.*, **24**, 185–188, https://doi.org/10.1029/96GL03953.

——, 2002: Effects of large-scale mountains on surface climate. A coupled ocean–atmosphere general circulation model study. *J. Meteor. Soc. Japan*, **80**, 1165–1181, https://doi.org/10.2151/jmsj.80.1165.

Kutzbach, J. E., W. L. Prell, and W. F. Ruddiman, 1993: Sensitivity of Eurasian climate to surface uplift of the Tibetan Plateau. *J. Geol.*, **101**, 177–190, https://doi.org/10.1086/648215.

Large, W. G., G. Danabasoglu, S. C. Doney, and J. C. McWilliams, 1997: Sensitivity to surface forcing and boundary layer mixing in a global ocean model: Annual-mean climatology. *J. Phys. Oceanogr.*, **27**, 2418–2447, https://doi.org/10.1175/1520-0485(1997)027<2418:STSFAB>2.0.CO;2.

Lawrence, D. M., and Coauthors, 2012: The CCSM4 land simulation, 1850–2005: Assessment of surface climate and new capabilities. *J. Climate*, **25**, 2240–2260, https://doi.org/10.1175/JCLI-D-11-00103.1.

Lee, S. S., J. Y. Lee, K. J. Ha, B. Wang, A. Kitoh, Y. Kajikawa, and M. Abe, 2013: Role of the Tibetan Plateau on the annual variation of mean atmospheric circulation and storm-track activity. *J. Climate*, **26**, 5270–5286, https://doi.org/10.1175/JCLI-D-12-00213.1.

Lowenstein, T. K., and R. V. Demicco, 2006: Elevated Eocene atmospheric CO_2 and its subsequent decline. *Science*, **313**, 1928, https://doi.org/10.1126/science.1129555.

Ma, Y. Z., J. J. Li, and X. M. Fang, 1998: Pollen assemblage in 30.6–5.0 Ma redbeds of Linxia region and climate evolution. *Chin. Sci. Bull.*, **43**, 301–304.

Maffre, P., J. B. Ladant, Y. Donnadieu, P. Sepulchre, and Y. Goddéris, 2018: The influence of orography on modern ocean circulation. *Climate Dyn.*, **50**, 1277–1289, https://doi.org/10.1007/s00382-017-3683-0.

Manabe, S., 1974: The effects of mountains on the general circulation of the atmosphere as identified by numerical experiments. *J. Atmos. Sci.*, **31**, 3–42, https://doi.org/10.1175/1520-0469(1974)031<0003:TEOMOT>2.0.CO;2.

Molnar, P., P. England, and J. Martinod, 1993: Mantle dynamics, uplift of the Tibetan Plateau, and the Indian monsoon. *Rev. Geophys.*, **31**, 357–396, https://doi.org/10.1029/93RG02030.

Naiman, Z., P. J. Goodman, J. P. Krasting, S. L. Malyshev, J. L. Russell, R. J. Stouffer, and A. T. Wittenberg, 2017: Impact of mountains on tropical circulation in two Earth system models. *J. Climate*, **30**, 4149–4163, https://doi.org/10.1175/JCLI-D-16-0512.1.

Nikurashin, M., and G. Vallis, 2012: A theory of the interhemispheric meridional overturning circulation and associated stratification. *J. Phys. Oceanogr.*, **42**, 1652–1667, https://doi.org/10.1175/JPO-D-11-0189.1.

Park, S., C. S. Bretherton, and P. J. Rasch, 2014: Integrating cloud processes in the Community Atmosphere Model, version 5. *J. Climate*, **27**, 6821–6856, https://doi.org/10.1175/JCLI-D-14-00087.1.

Rea, D. K., H. Snoeckx, and L. H. Joseph, 1998: Late Cenozoic Eolian deposition in the North Pacific: Asian drying, Tibetan uplift, and cooling of the Northern Hemisphere. *Paleoceanography*, **13**, 215–224, https://doi.org/10.1029/98PA00123.

Ruddiman, W. F., and J. E. Kutzbach, 1989: Forcing of late Cenozoic Northern Hemisphere climate by plateau uplift in southern Asia and the American West. *J. Geophys. Res.*, **94**, 18 409–18 427, https://doi.org/10.1029/JD094iD15p18409.

Schmittner, A., T. A. M. Silva, K. Fraedrich, E. Kirk, and F. Lunkeit, 2011: Effects of mountains and ice sheets on global ocean circulation. *J. Climate*, **24**, 2814–2829, https://doi.org/10.1175/2010JCLI3982.1.

Schneider, N., A. J. Miller, M. A. Alexander, and C. Deser, 1999: Subduction of decadal North Pacific temperature anomalies: Observations and dynamics. *J. Phys. Oceanogr.*, **29**, 1056–1070, https://doi.org/10.1175/1520-0485(1999)029<1056:SODNPT>2.0.CO;2.

Schott, F. A., J. P. McCreary, and G. C. Johnson, 2004: Shallow overturning circulations of the tropical–subtropical oceans. *Earth's Climate: The Ocean–Atmosphere Interaction, Geophys. Monogr.*, Amer. Geophys. Union, Vol. 147, 261–304, https://doi.org/10.1029/147GM15.

Seager, R., D. S. Battisti, J. Yin, N. Gordon, N. Naik, A. C. Clement, and M. A. Cane, 2002: Is the Gulf Stream responsible for Europe's mild winters? *Quart. J. Roy. Meteor. Soc.*, **128**, 2563–2586, https://doi.org/10.1256/qj.01.128.

Sepulchre, P., L. C. Sloan, M. Snyder, and J. Fiechter, 2009: Impacts of Andean uplift on the Humboldt Current system: A climate model sensitivity study. *Paleoceanography*, **24**, PA4215, https://doi.org/10.1029/2008PA001668.

Sinha, B., A. T. Blaker, J. J.-M. Hirschi, S. Bonham, M. Brand, S. Josey, R. S. Smith, and J. Marotzke, 2012: Mountain ranges favour vigorous Atlantic meridional overturning.

Geophys. Res. Lett., **39**, L02705, https://doi.org/10.1029/2011GL050485.

Smith, R. S., and J. M. Gregory, 2009: A study of the sensitivity of ocean overturning circulation and climate to freshwater input in different regions of the North Atlantic. *Geophys. Res. Lett.*, 36, L15701, https://doi.org/10.1029/2009GL038607.

Stephens, M., Z. Liu, and H. Yang, 2001: Evolution of subduction planetary waves with application to North Pacific decadal thermocline variability. *J. Phys. Oceanogr.*, **31**, 1733–1746, https://doi.org/10.1175/1520-0485(2001)031<1733:EOSPWW>2.0.CO;2.

Su, B., D. Jiang, R. Zhang, P. Sepulchre, and G. Ramstein, 2018: Difference between the North Atlantic and Pacific meridional overturning circulation in response to the uplift of the Tibetan Plateau. *Climate Past*, **14**, 751–762, https://doi.org/10.5194/cp-14-751-2018.

Toggweiler, J. R., and B. Samuels, 1995: Effect of Drake Passage on the global thermohaline circulation. *Deep-Sea Res. I*, **42**, 477–500, https://doi.org/10.1016/0967-0637(95)00012-U.

Valdes, P. J., and B. J. Hoskins, 1991: Nonlinear orographically forced planetary waves. *J. Atmos. Sci.*, **48**, 2089–2106, https://doi.org/10.1175/1520-0469(1991)048<2089:NOFPW>2.0.CO;2.

von der Heydt, A., and H. A. Dijkstra, 2006: Effect of ocean gateways on the global ocean circulation in the late Oligocene and early Miocene. *Paleoceanography*, **21**, PA1011, https://doi.org/10.1029/2005PA001149.

Wang, B., 2006: *The Asian Monsoon.* Springer, 787 pp.

Warren, B. A., 1983: Why is no deep water formed in the North Pacific? *J. Mar. Res.*, **41**, 327–347, https://doi.org/10.1357/002224083788520207.

Weaver, A. J., J. Marotzke, P. F. Cummins, and E. S. Sarachik, 1993: Stability and variability of the thermohaline circulation. *J. Phys. Oceanogr.*, **23**, 39–60, https://doi.org/10.1175/1520-0485(1993)023<0039:SAVOTT>2.0.CO;2.

White, R. H., D. S. Battisti, and G. H. Roe, 2017: Mongolian mountains matter most: Impacts of the latitude and height of Asian orography on Pacific wintertime atmospheric circulation. *J. Climate*, **30**, 4065–4082, https://doi.org/10.1175/JCLI-D-16-0401.1.

Woodruff, F., and S. M. Savin, 1989: Miocene deepwater oceanography. *Paleoceanography*, **4**, 87–140, https://doi.org/10.1029/PA004i001p00087.

Wu, G., 1999: The effect of spatially nonuniform heating on the formation and variation of sub-tropical high scale analysis. *Acta Meteor. Sin.*, **57**, 257–263.

——, Y. Liu, B. He, Q. Bao, A. Duan, and F. F. Jin, 2012: Thermal controls on the Asian summer monsoon. *Sci. Rep.*, **2**, 404, https://doi.org/10.1038/srep00404.

——, and Coauthors, 2015: Tibetan Plateau climate dynamics: Recent research progress and outlook. *Natl. Sci. Rev.*, **2**, 100–116, https://doi.org/10.1093/nsr/nwu045.

Wunsch, C., and R. Ferrari, 2004: Vertical mixing, energy, and the general circulation of the oceans. *Annu. Rev. Fluid Mech.*, **36**, 281–314, https://doi.org/10.1146/annurev.fluid.36.050802.122121.

Yang, H., and Q. Wen, 2019: Investigating the role of the Tibetan Plateau in the formation of Atlantic meridional overturning circulation. *J. Climate*, **33**, 3585–3601, https://doi.org/10.1175/JCLI-D-19-0205.1.

——, Q. Li, K. Wang, Y. Sun, and D. Sun, 2015: Decomposing the meridional heat transport in the climate system. *Climate Dyn.*, **44**, 2751–2768, https://doi.org/10.1007/s00382-014-2380-5.